Pergamon

Ocean Engng, Vol. 24, No. 5, pp. 445–464, 1997

0029-8018/97 $17.00 + 0.00

S0029-8018(96)00023-6

COUPLED DYNAMICS OF TETHERED BUOY SYSTEMS

K. Idris,* J. W. Leonard†§ and S. C. S. Yim‡

*Department of Civil Engineering, Bandung Institute of Technology, Bandung, Indonesia
†Department of Civil and Environmental Engineering, University of Connecticut, Storrs, CT 06269, U.S.A.
‡Ocean Engineering Program, Oregon State University, Corvallis, OR 97331, U.S.A.

(*Received* 6 *April* 1996; *accepted in final form* 15 *April* 1996)

Abstract—The three-dimensional coupled behavior during the interaction of buoys with their mooring systems is numerically analyzed. A time-domain model was developed to predict the response of a tethered buoy subject to hydrodynamic loadings. External loadings include hydrodynamic forces, tethers tensions, wind loadings and weight. System nonlinearities include large rotational and translational motions, and non-conservative fluid loadings. The mooring problem is formulated as a combined nonlinear initial-value and two-point-boundary-value problem which is directly integrated both in time and space. Buoy equations of motion are derived using small Eulerian angles. Coupling between rotational and translational degrees of freedom is included and coupling between the buoy and cable is effected by adopting the buoy equations of motion as boundary conditions at one end for the mooring problem. Numerical examples are provided to validate the formulation and solution technique; predicted responses of three types of buoy (sphere, spar, and disc) are compared with experimental results.

1. INTRODUCTION

The prediction of the three-dimensional kinetics and kinematics of a buoy-cable system is a complicated problem. The system behavior is highly nonlinear from the hydrodynamic and structural points of view. A coupled analysis is needed for this ocean structure, since motion of the buoy affects motion of the mooring and visa versa.

Numerical methods have been utilized to predict the motions of cable-buoy systems. The lumped parameter, e.g. Leonard and Nath (1981), and finite element, e.g. Webster (1975), methods require large memory capacities and long computation times. The direct integration method, e.g. Chiou and Leonard (1991), adopts a spatial integration scheme rather than spatial discretization and does not require extensive use of computer memory. Modelling of wave-body interactions depends on the size of the body relative to the incident wave length. A floating buoy with small characteristic dimensions may be analyzed by the generalized Morison equation (Morison *et al.*, 1950; Liaw *et al.*, 1989). Buoy dynamic equations were applied as boundary conditions for a mooring line by Nath and Thresher (1975). Patel and Lynch (1983) studied coupled dynamics of a tension buoyant platform with its mooring tethers; the small rotation assumption for platform motions was used and nonlinearities due to drag-induced viscous damping were included in an iterative analysis.

A numerical procedure is presented in the next section to solve the de-coupled cable

§Corresponding author.

problem, in which the problem is formulated as a two point boundary value problem. In the third section the nonlinear equations of motion for the buoy are developed and converted to a form that can be incorporated as boundary conditions in the cable algorithm. Only bodies with axisymmetric geometries are considered in this study; nonsymmetric loadings and responses are admitted, however. Analysis is performed in three dimensions so that all three translational degrees of freedom (heave, surge, and sway) and all three rotational degrees of freedom (yaw, roll, and pitch) are considered. The buoy is considered small compared to the incident wave length. An algorithm is developed in a subsequent section for quasi-linearization of those boundary conditions for use in determining the tether motions and buoy rotations for the coupled nonlinear system. Comparisons of computational results with experimental data are provided in the fifth section.

2. CABLE DYNAMICS

The dynamics of the cable are modeled using a numerical algorithm for a hydrodynamically loaded cable problem previously developed by Chiou and Leonard (1991). A summary of the algorithm is presented here in order to explain the methodology used to combine the cable and buoy systems. Figure 1 shows the general definition sketch for the system of cable and body components. A fixed (global) coordinate system is defined with the origin at the still water line; S_0 is the cable local coordinate along the cable scope; and O is an arbitrary material point on the cable at a distance S from one end of the cable. The cartesian components of the position of an arbitrary point on the cable at time t are defined as $x_i(S_0,t)$ and the tension components as $T_i(S_0,t)$, where i ranges from 1 to 3.

The cable is under hydrodynamic loading from surface waves and subsurface currents. The cable governing equations were derived from the equilibrium of dynamic forces on an infinitesimal length of cable dS at an arbitrary point O along the cable segment. Hydrodynamic loading per unit length includes buoyancy, added mass forces and drag forces.

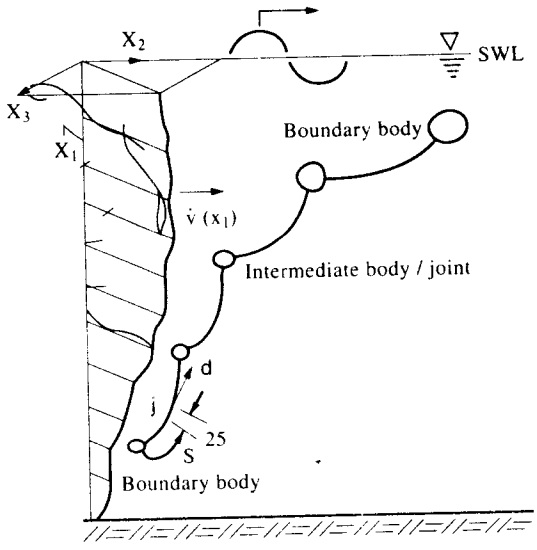

Fig. 1. Cable general definition sketch (Chiou and Leonard, 1991).

The strain ϵ is assumed to be small and the cable governing equations can then be written, in indicial notation, as

$$\frac{dx_i}{dS_0} = (1 + \epsilon)\frac{T_i}{T} \tag{1}$$

$$\frac{dT_i}{dS_0} = -\alpha_1(1 + \epsilon)Q^nQ_i^n - \alpha_2(1 + \epsilon)Q^tQ_i^t - \alpha_3(1 + \epsilon)\dot{u}_i^n + \alpha_4(1 + \epsilon)\dot{u}'^n_i - W_b\delta_{i1} + m\ddot{x}_i \tag{2}$$

where

$$\alpha_1 = 0.5\rho DC_D^a$$

$$\alpha_2 = 0.5\rho DxC_d^t$$

$$\alpha_3 = 0.25\rho D_2(C_A + 1)$$

$$\alpha_4 = 0.25\rho\pi D^2C_a$$

$$Q_i^n = (\dot{u}_k + \dot{v}_k - \dot{x}_k)\left(\delta_{ik} - \frac{T_iT_k}{T^{2\prime}}\right)$$

$$Q_i^t = (\dot{u}_k + \dot{v}_k - \dot{x}_k)\left(\frac{T_iT_k}{T^2}\right)$$

$$Q^n = \sqrt{Q_k^nQ_k^n}$$

$$Q^t = \sqrt{Q_k^tQ_k^t}$$

$$\dot{u}'^n_i = \dot{u}'_k\left(\delta_{ik} - \frac{T_iT_k}{T^2}\right)$$

$$\ddot{x}_i^n = \ddot{x}_k\left(\delta_{ik} - \frac{T_iT_k}{T^2}\right)$$

$$T = \sqrt{T_iT_i} = \text{ magnitude of tension}$$

in which the superscripts t and n denote vector components tangential and normal to the cable axis, m is mass density of the cable, C_A is the added mass coefficient, $C_D{}^n$ and $C_D{}^t$ are normal and tangential drag coefficients, respectively, and δ_{ik} = kronecker delta = 0 if $i \neq k$ or = 1 if $i = k$.

The cable governing equations of motion are second order partial differential equations with independent variables time, t and cable unstretched length, S_0. For a three-dimensional space a set of six second order equations is obtained which can be transformed into a set of twelve first order differential equations. Introducing cable velocity

$$\frac{\partial x_i}{\partial t} = \dot{x}_i \tag{3}$$

Equation (2) can then be written as

$$\frac{\partial T_i}{\partial S_0} = -\alpha_1(1+\epsilon)Q^nQ_i^n - \alpha_2(1+\epsilon)Q^tQ_i^t - \alpha_3(1+\epsilon)\dot{u}_i^n \tag{4}$$

$$+ \alpha_4(1+\epsilon)\frac{\partial \dot{x}_i^n}{\partial t} - W_b\delta_{1i} + m\frac{\partial \dot{x}_i}{\partial t}$$

Taking the derivative of Equation (3) with respect to S_0

$$\frac{\partial \dot{x}_i}{\partial S_0} = \frac{\partial}{\partial t}\frac{\partial x_i}{\partial S_0} \tag{5}$$

and substituting Equation (1) into Equation (5), one obtains

$$\frac{\partial \dot{x}_i}{\partial S_0} = \frac{\partial}{\partial t}\left[(1+\epsilon)\frac{T_i}{T}\right] = \frac{T_i}{T}\frac{\partial \epsilon}{\partial t} - (1-\epsilon)\sqrt{1-\left(\frac{T_i}{T}\right)^2}\frac{\partial}{\partial t}\left[\cos^{-1}\frac{T_i}{T}\right] \tag{6}$$

Now, the cable governing equations are given as Equation (4) and Equation (6), in which new dependent variables of velocity components, $\dot{x}_i$ are introduced. This set of equations constitutes a combined boundary-value and initial-value problem because of time evolution. The initial conditions for the problem are required to be specified in term of S_0 and two sets of boundary conditions are also needed on each cable end at each instant in time. Approximation of the time derivatives can be made using an implicit Newmark-like formula (Newmark, 1959; Clough and Penzien, 1993). This approach converts the problem to a discrete two-point boundary-value problem at each instant in time. The difference equations for time derivatives can be written at time t in terms of values at a previous time t'' and time step $\delta t = t - t''$ as

$$\frac{\partial \epsilon}{\partial t} = \frac{1}{\alpha\Delta t}(\epsilon - \epsilon'') - \gamma\left(\frac{\partial \epsilon}{\partial t}\right)'' \tag{7}$$

$$\frac{\partial}{\partial t}\cos^{-1}\left(\frac{T_i}{T}\right) = \frac{1}{\alpha\Delta t}\left[\cos^{-1}\left(\frac{T_i}{T}\right) - \cos^{-1}\left(\frac{T_i''}{T''}\right)\right] - \gamma\left[\frac{\partial}{\partial t}\cos^{-1}\left(\frac{T_i}{T}\right)\right]'' \tag{8}$$

$$\frac{\partial \dot{x}}{\partial t} = \frac{1}{\alpha\Delta t}(\dot{x}_i - \dot{x}_i'') - \gamma\ddot{x}'' \tag{9}$$

where $\delta=(1-\alpha)/\alpha$ and ϵ'', T'', T_i'' and $\dot{x}_i''$ are values of ϵ, T, T_i and $\dot{x}_i$ at time t''.

This set of nonlinear discrete equations poses a two-point boundary value problem in the spatial coordinate S_0. They can be converted to an iterative set of linear boundary-value problems using the Newton–Raphson method (Atkinson, 1989). The quasi-linearized two point boundary-value problems can then be further decomposed into a set of initial-value problems so that a trial solution can be integrated numerically from one end to the other.

In decomposing the boundary value problem into a set of initial-value problems, one may express the solution as a linear combination of homogenous solutions (${}^j\dot{x}_i$ and ${}^jT_i$) and a particular solution (${}^\circ\dot{x}_i$ and ${}^\circ T_i$) as

$$\dot{x}_i = {}^\circ\dot{x}_i + \alpha_j{}^j\dot{x}_i \tag{10}$$

$$T_i = {}^\circ T_i + \alpha_j{}^jT_i \tag{11}$$

where α_j are undetermined coefficients to recombine solutions. Initial values that satisfy the actual boundary condition can be specified for each initial-value problem.

Solution of the boundary value problem is obtained by successive iteration. In each iteration, particular and homogenous cable equations are integrated from the starting point to the terminal point at the other end of the cable. Knowing the boundary condition at the terminal end, one can evaluate the partial solution to obtain the appropriate coefficients α_j for the linear combination of partial solutions at the starting end or to obtain the new iterates to x_{T_i} and T_i.

The model has capabilities to solve problems with stationary or moving boundary conditions and force boundary conditions. For the mooring problem, the starting end of the mooring cable may be held stationary (zero velocity) at the ocean floor

$$\dot{x}_i(t) = 0 \tag{12}$$

At the other end a floating buoy may be attached; in this case the equations of motion for the tethered floating buoys serve as boundary conditions.

3. BUOY DYNAMICS

The buoy equations of motion constitute the boundary conditions for one end of the mooring tether. A definition sketch of a buoy floating on the moving water surface and connected by a tether to the ocean bottom is depicted in Fig. 2. Two cartesian coordinate systems are defined, a moving (local) coordinate system attached to the buoy, and a fixed (global) coordinate system with the origin at the mean water line.

The origin of the buoy/local coordinate is located at point G, the center of mass for the buoy. Point T is the location of the tether connection point and z_T is the local position vector to T from G. Point W is the location of application of point loads from external sources, e.g., wind, and z_W is the local position vector to W from G. Point B is the location of the center of buoyancy and is the point at which resultant hydrodynamic loads are assumed to be applied and z'_B is the local position vector to B from G.

The motion of the buoy can be characterized by the translation vector of the point G,

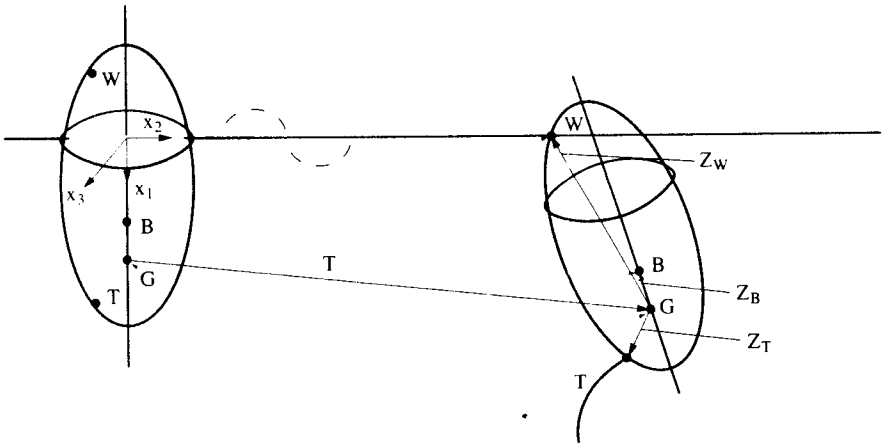

Fig. 2. Definition sketch of buoy vectors.

$r^T = \{x_1, x_2, x_3\}^T$ and the rotational vector of the buoy around its center of gravity G, $I^T = \{I_1, I_2, I_3\}^T$. The rotation vector I is assumed to be small enough that as the buoy moves from an initial static equilibrium position to a position at time t, the position vector r_P of an arbitrary point P in the buoy can be written as

$$r_P = \underline{r} + \underline{s}_P' + \underline{\theta} \times \underline{s}_P' \tag{13}$$

where r is the translational motion of point G and s_P' is the local position vector to P from G. Then, the acceleration and velocity at a general point P on the buoy can be obtained from time derivatives of Equation (13).

$$\ddot{r}_P = \ddot{\underline{r}} + \ddot{\underline{\theta}} \times \underline{s}_P' \tag{14}$$

$$\dot{r}_P = \dot{\underline{r}} + \dot{\underline{\theta}} \times \underline{s}_P' \tag{15}$$

3.1. *Buoy kinetics*

The vector sum of the forces acting on the buoy and of their moments about point G must equal the inertial force and moment vectors for the buoy, $\boldsymbol{M}\ddot{q}$. Where $\boldsymbol{M}$ is the generalized mass and added mass matrix for the buoy, and $\ddot{\underline{q}}^T = \{\ddot{\underline{r}}^T \ddot{\underline{\theta}}^T\}$ is the acceleration of the center of gravity. Thus

$$\boldsymbol{M}\ddot{\underline{q}} = \begin{Bmatrix} \underline{F}_W \\ \underline{N}_W \end{Bmatrix} - \begin{Bmatrix} \underline{T} \\ \underline{N}_T \end{Bmatrix} + \begin{Bmatrix} \underline{W}_{\mathrm{DRY}} \\ \underline{0} \end{Bmatrix} + \begin{Bmatrix} \underline{B} \\ \underline{N}_B \end{Bmatrix} + \begin{Bmatrix} \underline{F}_d \\ \underline{N}_d \end{Bmatrix} + \begin{Bmatrix} \underline{F}_K \\ \underline{N}_K \end{Bmatrix} \tag{16}$$

in which the force vectors are: buoy dry weight $\underline{W}_{\mathrm{DRY}}$, buoyancy $\underline{B}$, hydrodynamic inertia force $\underline{F}_I$, hydrodynamic drag force $\underline{F}_D$, the Froude–Kryloff force $\underline{F}_K$, wind or other external force $\underline{F}_W$, and tether tension $\underline{T}$ at the tether connection point. The wind or other external force is given as a concentrated load which may vary with time. The buoy is assumed small compared to incident wave lengths. Thus, the added mass coefficient may be taken as frequency independent and radiation damping neglected.

The external moment of forces is evaluated about the center of gravity, and can be expressed as

$$\underline{N}_P = \underline{s}'_P \times \underline{F}_P \tag{17}$$

where $\underline{F}_P$ is an external force and $\underline{s}'_P$ is the point of application of the external force on the buoy, in the local coordinate system. The resultant of hydrodynamic loads on the buoy is assumed to be applied at the center of buoyancy, the location of which depends on buoy submergence. Small angular displacements are assumed. In this formulation the center of rotation is assumed to be at the center of gravity. Components of individual matrices and vectors are given in the Appendix.

Equation (16) constitutes six non-linear second-order differential equations of motion for the six degrees of freedom r and $\underline{I}$ in terms of the external and fluid forces applied to the buoy and the tether forces restraining the buoy.

The equations of motion may be separated into translational and rotational components. Since velocity and acceleration of the tether connection can be obtained from the cable algorithm, one may express $\dot{\underline{r}}$ and $\ddot{\underline{r}}$ in terms of velocity and acceleration at the tether point T using Equation (14) and Equation (15). Thus, the buoy equations of motion may be written, in indicial notation, as

$$-(M_{(i)} + \rho V_{wet} C_{A(i)(i)})(\ddot{x}_{Ti} - \epsilon_{ijk} z_{Tk} \ddot{\theta}_j) - \rho V_{wet} C_{A(i)(j+3)} \ddot{\theta}_j + F_{wi} - T_i$$
$$+ (M_{(1)} - \rho V_{wet}) g \delta_{1j} + (1 + C_{A(i)(i)}) \rho V_{wet} \dot{V}_i \tag{18}$$
$$+ N_{D(i)}(V_i - \dot{x}_{Ti} - \epsilon_{ijk} z_{TBk} \dot{\theta}_j) = 0$$

$$-[I_{ij} + C_{A(i+3)(j+3)} \rho V_{wet}] \ddot{\theta}_j - \rho V_{wet} C_{A(i+3)(j)} [\ddot{x}_{Ti} - \epsilon_{ijk} z_{Tk} \ddot{\theta}_j]$$
$$- [N_{D(j)} W_{ij}] \dot{x}_{Tj} - [\epsilon_{kjn} N_{D(k)} z_{Bn} W_{ik}] \dot{\theta}_j + [z_{Wi} F_{Wj} - z_{Ti} T_j - z_{Bi} B_j \delta_{1j} \tag{19}$$
$$- \delta_{ij}(z_{Wk} F_{Wk} - z_{Tk} T_k - z_{Bk} B_k \delta_{1k})] \theta_j + \epsilon_{ijk}[z_{Wj} F_{Wk} - z_{Tj} T_k - M_{Fjk}]$$
$$- \rho g I_{wp}(\theta_j - \zeta_j) = 0$$

where

$$W_{ik} = \epsilon_{ink} z_{Bn} + z_{Bi} \theta_k - z_{Bk} \theta_i \tag{20}$$

$$M_{Fik} = (z_{Bi} + C_{A(i+3)(k)}) \rho V_{wet} \dot{V}_k + (N_{D(k)} \dot{V}_k - \rho g V_{wet} \delta_{1k}) z_{Bi} \tag{21}$$

and the magnitude of relative velocity at point B and the distance from T to B are

$$z_{TBi} = z_{Bi} - z_{Ti} \tag{22}$$

$$Q = [\ (V_i - \dot{x}_{Ti} - \epsilon_{ijk} z_{TBk} \dot{\theta}_j)\ (V_i - \dot{x}_{Ti} - \epsilon_{imn} z_{TBn} \dot{\theta}_m)\ ]^{1/2} \tag{23}$$

These equations of motion can be incorporated with the cable algorithm by applying them as boundary conditions at the terminal end of the cable. The translational components of the equation of motion serve as three boundary conditions for the tether point tensions and translational velocities at tether connection point T; the rotational components serve as three auxiliary differential equations for the buoy rotations I.

4. SOLUTION ALGORITHM

Equations (18) and (19) are second-order ordinary differential equations in time which serve as boundary conditions at the terminus of the cable. To implement these boundary conditions, these equations can be converted into discrete equations by a Newmark-like implicit integration scheme as performed on the cable algorithm. Accelerations at time $t = t' + \Delta t$ are approximated as

$$\ddot{x}_{Ti} = (\dot{x}_{Ti} - \dot{x}''_{Ti})/(\alpha \Delta t) - \gamma \ddot{x}''_{Ti} \tag{24}$$

$$\ddot{\theta}_i = (\dot{\theta}_i - \dot{\theta}''_i)/(\alpha \Delta t) - \gamma \ddot{\theta}''_i \tag{25}$$

where $\delta = (1-\alpha)/\alpha$ and $\alpha = 1/2$ for implicit integration, and x_{Ti}'', $\dot{x}_{Ti}''$, $\ddot{x}_{Ti}''$, I_i'', θ_i'', $\dot{\theta}_i''$ $\ddot{\theta}_i''$ are known values at a prior time step t''. The translational and rotational displacements can be expressed, using the same formulation, as

$$x_{Ti} = \alpha \Delta t(\dot{x}_{Ti} + \gamma \dot{x}_{Ti}'') + x_{Ti}'' \tag{26}$$

$$\theta_i = \alpha \Delta t(\dot{\theta}_i + \gamma \dot{\theta}_i'') + \theta_i'' \tag{27}$$

Then, upon substitution of Equation (24) through Equation (27) into Equation (18) and Equation (19), quasi-static nonlinear equations at time t are obtained.

The nonlinear quasi-static equations obtained from Equation (18) and Equation (19) with approximate time derivatives Equation (24) through Equation (27) are the nonlinear

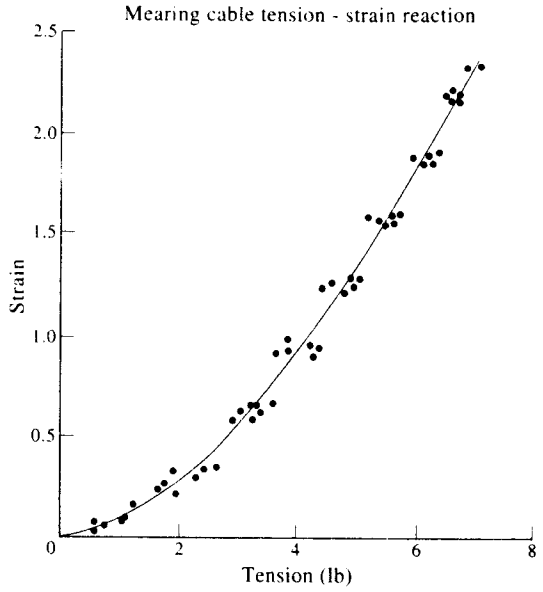

Fig. 3. Tension-strain relationship for mooring cable.

boundary conditions for the tether attached to point I. Those conditions are written here in functional form as

$$f_i(T_j,\ x_{Tj},\ \theta_j) = 0 \tag{28}$$

$$h_i(T_j,\ x_{Tj},\ \theta_j) = 0 \tag{29}$$

where f_i describes force equilibrium and h_i describes moment equilibrium. To incorporate

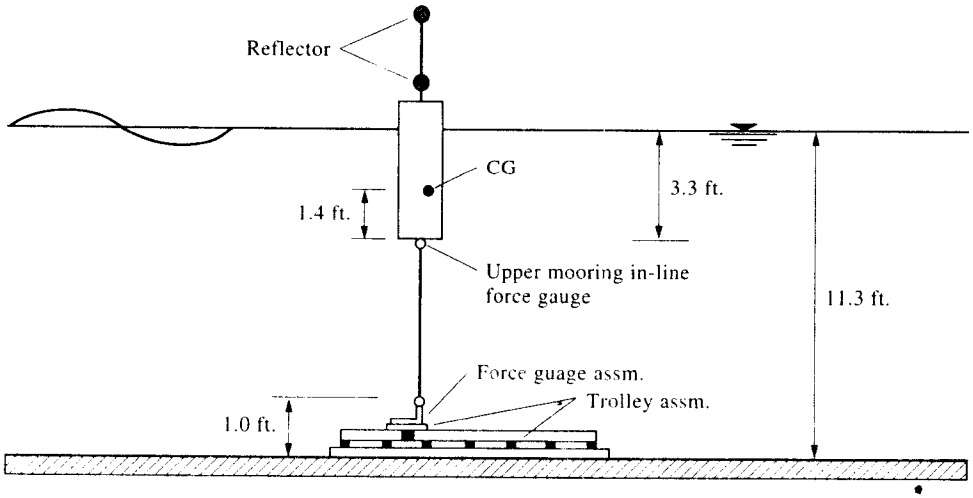

Fig. 4. Configuration of spar buoy test.

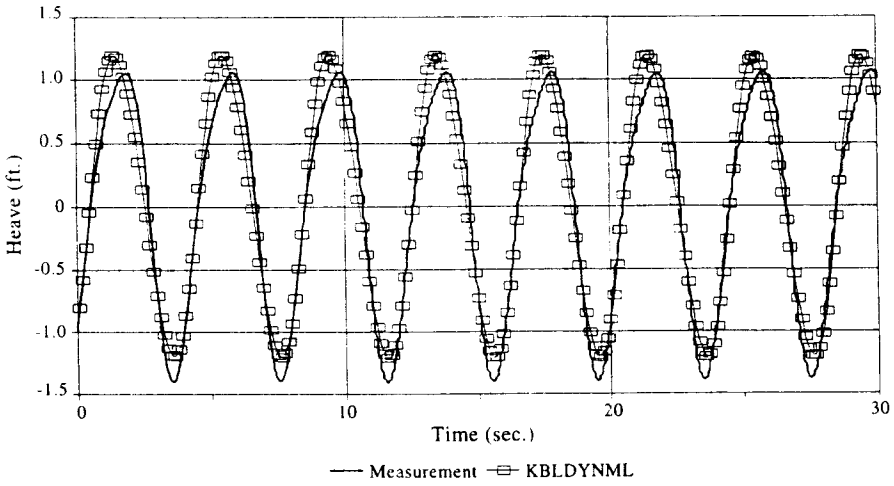

Fig. 5. Heave displacement, spar buoy. H=2.5 ft, T=4.0 sec.

these equations with the cable algorithm the nonlinear quasi-static equations need to be quasi-linearized by the Taylor expansion. The Newton–Raphson method can then be used to determine improved estimates T_i, $\dot{x}_{Ti}$ and $\dot{\theta}_i$, given prior estimates T_i'', $\dot{x}_{Ti}''$ and $\dot{\theta}_i''$. Taking Taylor series expansions of the difference equations f_i and h_i from Equation (18) and Equation (19) about the functions f_i^* and h_i^* evaluated at T_i^*, x_{Ti}^* and $\dot{\theta}_i^*$ with respect to increments $(T_i - T_i^*)$, $(\dot{x}_{Ti} - \dot{x}_{Ti}^*)$, and $(\dot{\theta}_i - \dot{\theta}_i^*)$, one writes

$$f_i = 0 = f_i^* + J_{Fxij}^*(\dot{x}_{Tj} - \dot{x}_{Tj}^*) + J_{FTij}^*(T_j - T_j^*) + J_F^*\theta_{ij}(\dot{\theta}_j - \dot{\theta}_j^*) \tag{30}$$

$$h_i = 0 = h_i^* + J_{Hxij}^*(\dot{x}_{Tj} - \dot{x}_{Tj}^*) + J_{HTij}^*(T_j - T_j^*) + J_H^*\theta_{ij}(\dot{\theta}_j - \dot{\theta}_j^*) \tag{31}$$

Components of the Jacobian matrices J_{Fxij}^*, J_{FTij}^*, J_{FIij}^*, J_{Hxij}^*, J_{HTij}^*, and J_{HIij}^* are written in the Appendix.

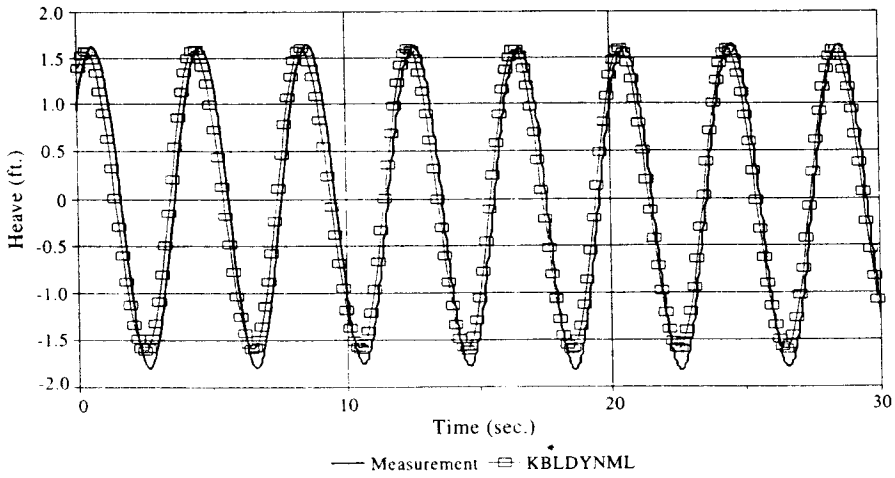

Fig. 6. Surge displacement, spar buoy, H=2.5 ft, T=4.0 sec.

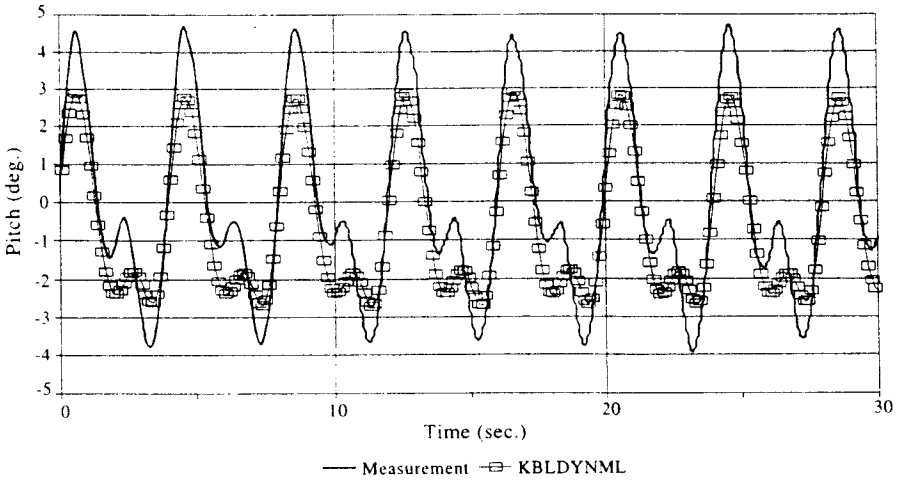

Fig. 7. Pitch displacement, spar buoy, H=2.5 ft, T=4.0 sec.

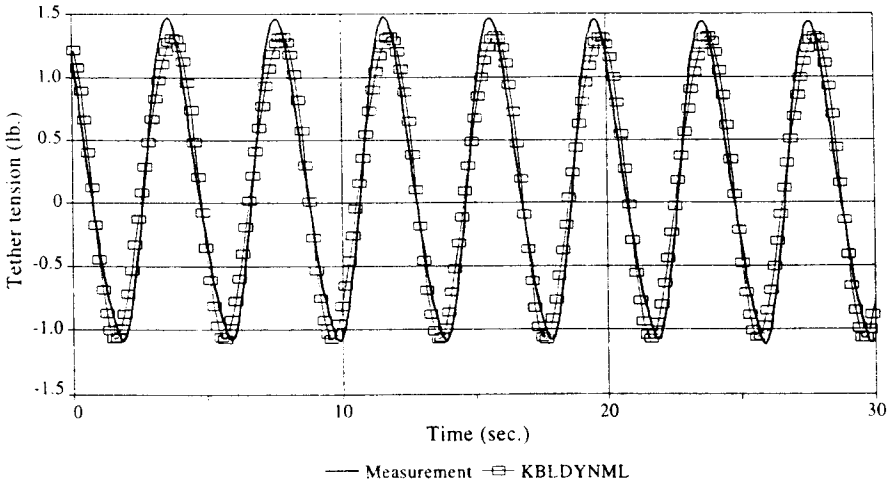

Fig. 8. Tether tension, spar buoy, H=2.5 ft, T=4.0 sec.

Equation (30) and Equation (31) are six linear algebraic equations for nine unknowns T_i, $\dot{x}_{Ti}$ and θ_i in terms of prior estimates T_i^*, $\dot{x}_{Ti}^*$ and θ_i^*. The six unknowns T_i, $\dot{x}_{Ti}$ are related to the three boundary conditions at the starting end of the tether through the cable differential equations. The unknown x_{Ti} and T_i at the tether point are decomposed into homogenous and particular solutions as in Equation (10) and Equation (11). Upon substitution of Equation (10) and Equation (11), one obtains six equations to be solved for six unknowns α_i and $\dot{\theta}_i$. Equation (30) and Equation (31) can be written in matrix form as

$$\begin{bmatrix} \boldsymbol{K}_{FF}^* & \boldsymbol{K}_{F\theta}^* \\ \boldsymbol{K}_{\theta F}^* & \boldsymbol{K}_{\theta\theta}^* \end{bmatrix} \begin{Bmatrix} \underline{\alpha} \\ \underline{\dot{\theta}} \end{Bmatrix} = \begin{Bmatrix} \underline{P_F^*} \\ \underline{P_\theta^*} \end{Bmatrix} \quad \bullet (32)$$

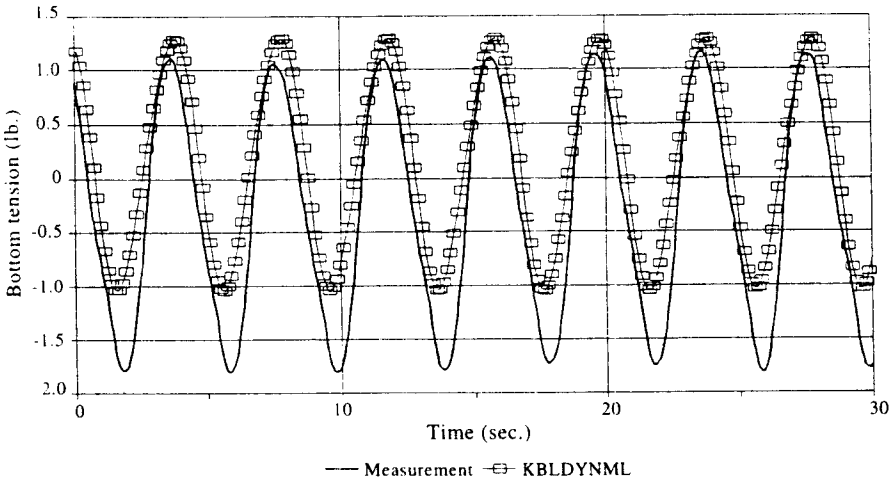

Fig. 9. Bottom tension, spar buoy, H=2.5 ft, T=4.0 sec.

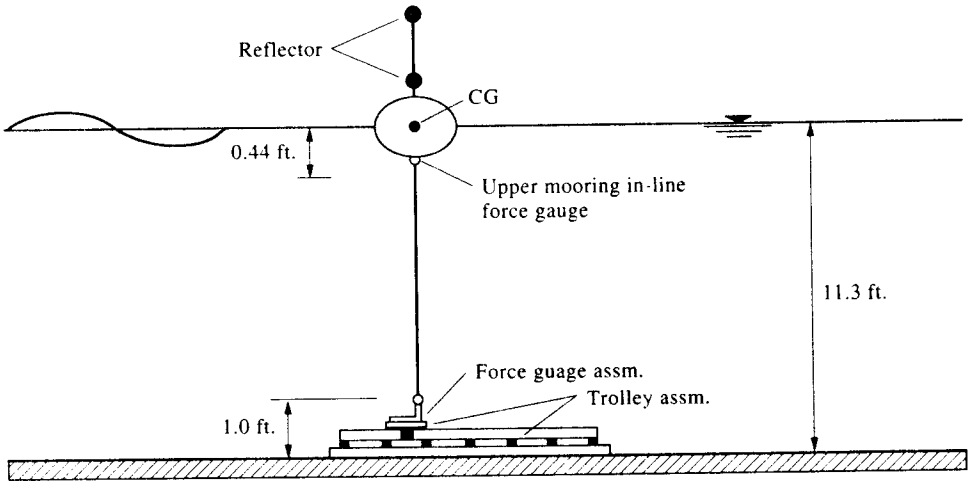

Fig. 10. Configuration of sphere buoy test.

where the submatrices are given by

$$\boldsymbol{K}^*_{FF} = [J^*_{Fxik}][\{^1\dot{x}_{Tj}\},\ \{^2\dot{x}_{Tj}\},\ \{^3\dot{x}_{Tj}\}] + [J^*_{FTik}][\{^1T_j\},\ \{^2T_j\},\ \{^3T_j\}] \tag{33}$$

$$\boldsymbol{K}^*_{\theta F} = [J^*_{Hxik}][\{^1\dot{x}_{Tj}\},\{^2\dot{x}_{Tj}\},\{^3\dot{x}_{Tj}\}] + [J^*_{HTik}][\{^1T_j\},\{^2T_j\},\{^3T_j\}] \tag{34}$$

$$\boldsymbol{K}^*_{F\theta} = [J^*_F\theta_{ik}] \tag{35}$$

$$\boldsymbol{K}^*_{\theta\theta} = [J^*_H\theta_{ij}] \tag{36}$$

$$\underline{P}^*_F = -\{f^*_i\} + [J^*_{Fxij}](\{\dot{x}^*_{Tj}\} - \{^\circ\dot{x}_{Tj}\}) + [J^*_{FTij}](\{T^*_j\} - \{^\circ T_j\}) + [J^*_F\theta_{ij}]\{\dot{\theta}^*_j\} \tag{37}$$

$$\underline{P}^*_\theta = -\{h^*_i\} + [J^*_{Hxij}](\{\dot{x}^*_{Tj}\} - \{^\circ\dot{x}_{Tj}\}) + [J^*_{HTij}](\{T^*_j\} - \{^\circ T_j\}) + [J^*_H\theta_{ij}]\{\dot{\theta}^*_j\} \tag{38}$$

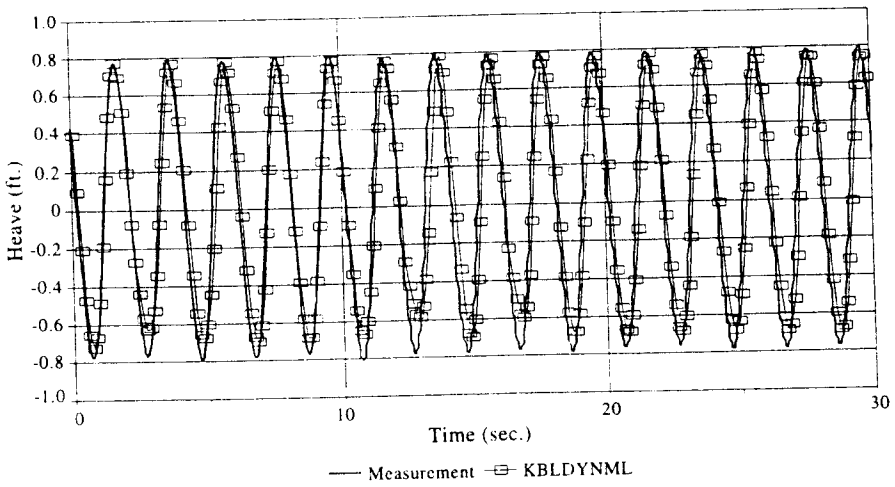

Fig. 11. Heave displacement, sphere buoy H=1.5 ft, T=2.0 sec.

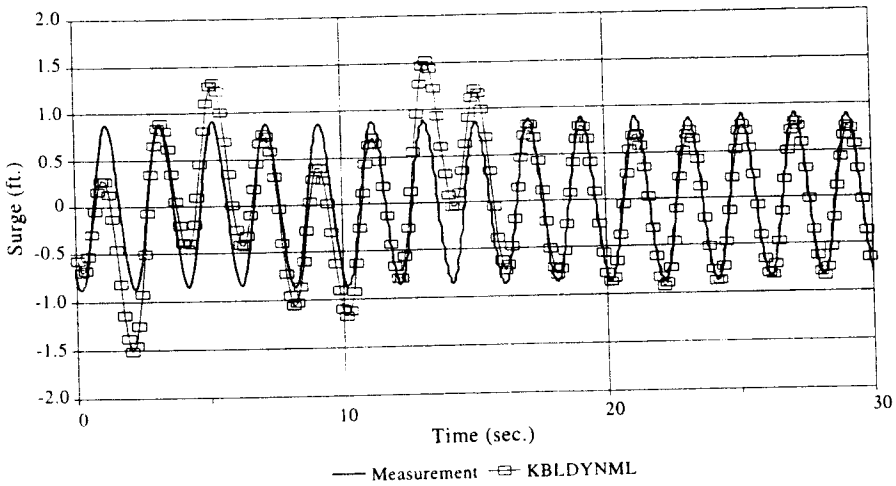

Fig. 12. Surge displacement, sphere buoy, H=1.5 ft, T=2.0 sec.

The solutions algorithm proceeds as follows:

1. Given a solution at time t'' to the tether variables T_i'', $\dot{x}_{Ti}''$ at all cable points, in particular T_i'', $\dot{x}_{Ti}''$ and $\dot{\theta}_i''$ at the buoy, extrapolate an initial estimate of T_i^*, $\dot{x}_{Ti}^*$ and $\dot{\theta}_i''$ at time t.
2. Integrate the partial particular and homogenous cable equations from the bottom boundary condition to the buoy.
3. Form matrices in Equation (32) and solve for α_i and $\dot{\theta}_i$.
4. Combine partial solutions using α_i and compare T_i, $\dot{x}_{Ti}$ and $\dot{\theta}_i$ to estimate T_i^*, $\dot{x}_{Ti}^*$ and $\dot{\theta}_i^*$.
5. If sufficient convergence is achieved, set $T_i'' = T_i$, $\dot{x}_{Ti}'' = \dot{x}_{Ti}$, $\dot{\theta}_i'' = \dot{\theta}_i$ and return to step 1; if convergence is not achieved, set $T_i^* = T_i$, $\dot{x}_{Ti}^* = \dot{x}_{Ti}$, $\dot{\theta}_i^* = \dot{\theta}_i$ and return to step 2.

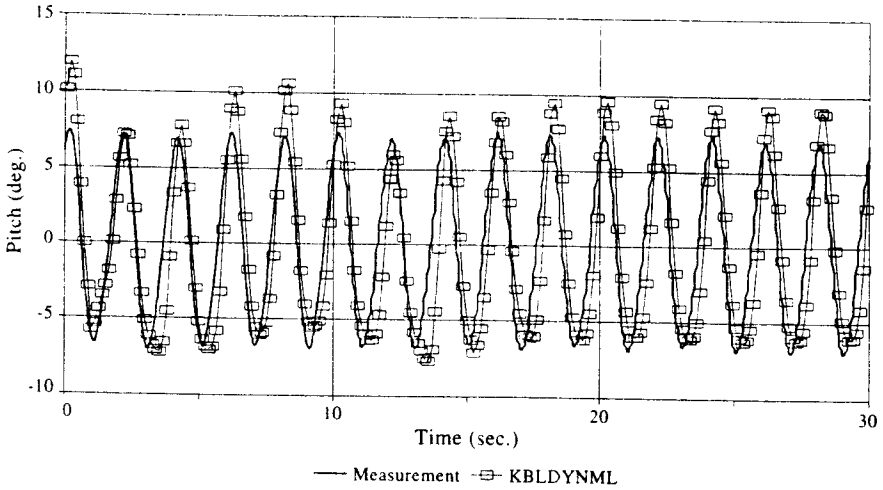

Fig. 13. Pitch displacement, sphere buoy H=1.5 ft, T=2.0 sec.

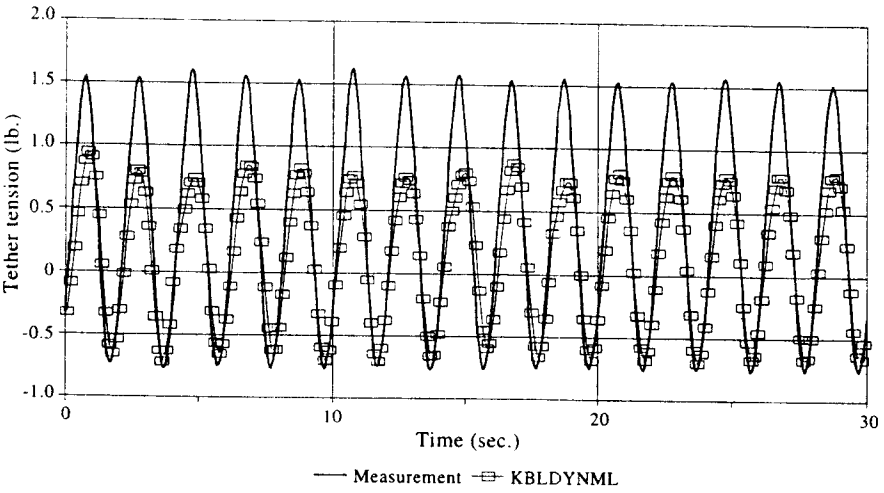

Fig. 14. Tether tension, sphere buoy H=1.5 ft, T=2.0 sec.

5. COMPARISON WITH EXPERIMENTAL RESULTS

To validate the simulation method, comparisons between numerical model predictions and experimental results were performed. Three cable-buoy systems were simulated and comparisons made with experimental results taken from selected buoy tests conducted at the Oregon State University O. H. Hinsdale Wave Research Laboratory in April 1992. Details of the experimental set up and data collection methods are described in Jenkins *et al.* (1995).

The three models tested were a spar buoy, a sphere buoy and a disc buoy. For all simulations, the mooring line is a 5/16 in. surgical rubber tube, with 2.41 ft initial mooring length. A simple tensile test was performed to obtain a strain-tension relation of the

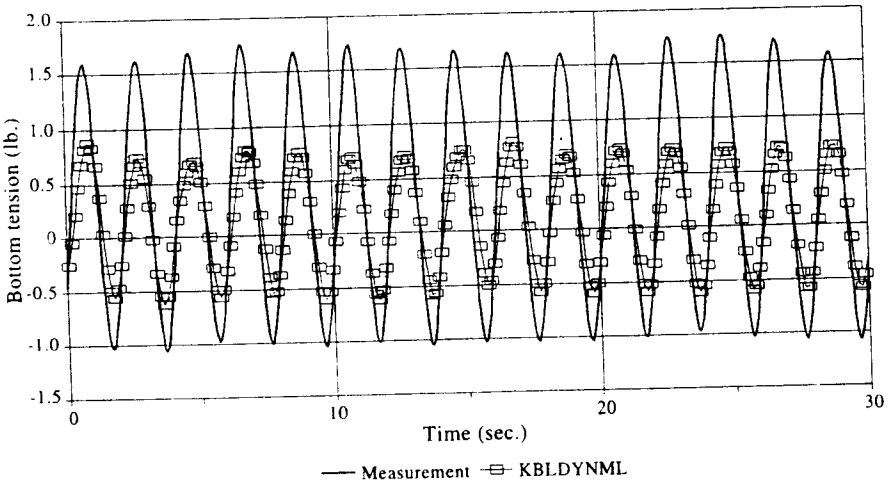

Fig. 15. Bottom tension, sphere buoy H=1.5 ft, T=2.0 sec.

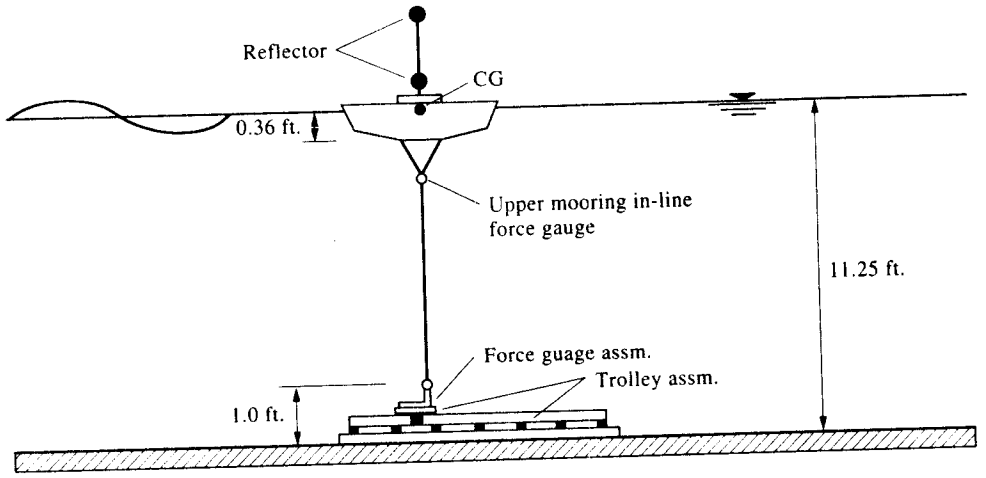

Fig. 16. Configuraton of disc buoy test.

rubber tube mooring; the tension-strain curve for this material is shown in Fig. 3. The experimental data were recovered at 30 Hz; thus a time increment of 0.066 sec. was selected to match the time increment on the experimental data. A stream function wave theory was used to simulate the generated wave. An initial 30 sec. duration ramp of wave amplitude was used to start the simulation from rest. Each case was run for a total of 100.0 sec.; the last 50 sec. of computational results, by which time the system has reached a steady state condition, are used for comparison.

The first comparison is for a 6.35 in. diameter, 50 in. tall and 45.3 lb weight spar buoy. The loading is a monochromatic wave train 2.5 ft high with a 4.0 sec. period. A definition sketch for this problem is shown in Fig. 4. The comparison of the predicted and measured response are shown in Figs 5–9. Predicted translational displacements agree

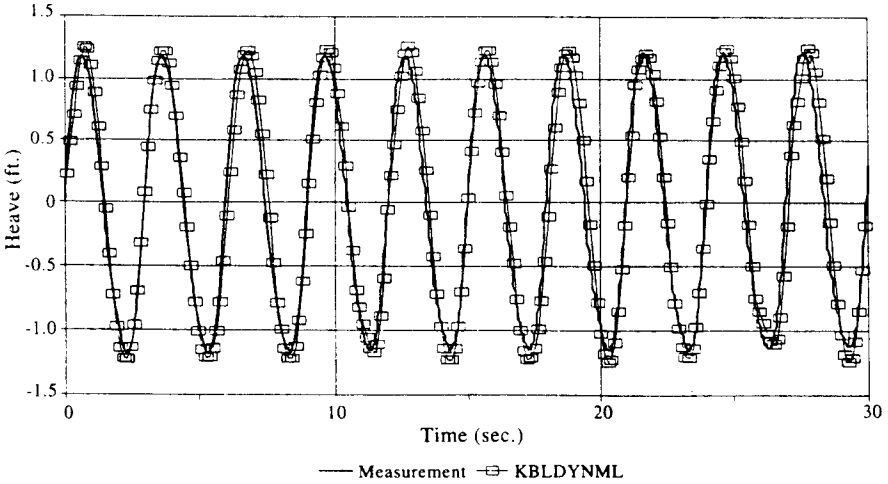

Fig. 17. Heave displacement, disc buoy, H=2.5 ft, T=3.0 sec.

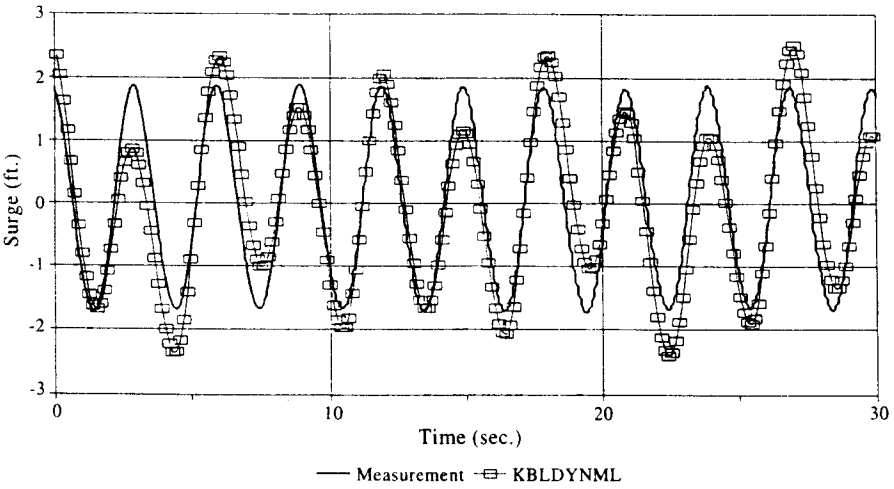

Fig. 18. Surge displacement, disc buoy, H=2.5 ft, T=3.0 sec.

well with measurements; predicted rotational motions do not agree as well, but have the same quantitative form. The dynamic components of tension at the tether and at the bottom connection differ from experimental values; tensions are under-predicted because of visco-elastic behavior of the rubber mooring line which was not simulated by the nonlinear elastic cable model.

The second comparison is a sphere buoy with 13.5 in. diameter and 17.1 lb dry weight. The loading is a monochromatic wave train 1.5 ft high with a 2.0 sec. period. A definition sketch for this problem is shown in Fig. 10. The comparison of the predicted and measured responses are shown in Figs 11–15. The predicted translational motions are close to the experimental results at the steady state condition near the end of the record. Pitch displacements are overpredicted and tensions underpredicted.

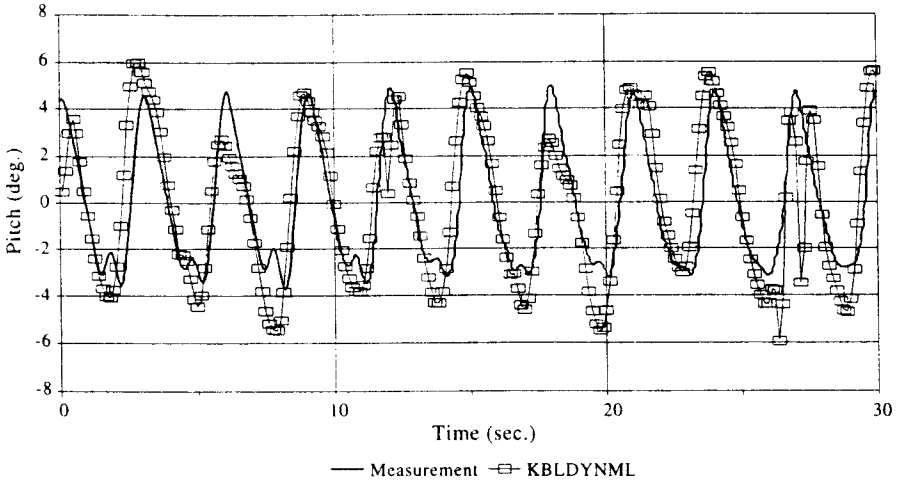

Fig. 19. Pitch displacement, disc buoy H=2.5 ft, T=3.0 sec.

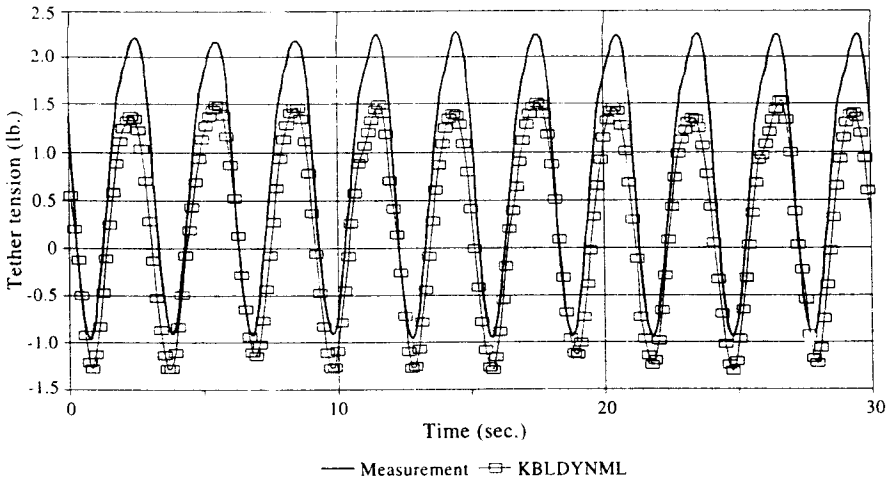

Fig. 20. Tether tension, disc buoy H=2.5 ft, T=3.0 sec.

The last comparison is for a 22 in. diameter, 6 in. deep and 21.4 lb weight disc buoy which is a commonly used NDBC buoy model. The loading is a monochromatic wave train 2.5 ft high with a 3.0 sec. period. A definition sketch for this problem is shown in Fig. 16. The comparison of the predicted and measured responses are shown in Figs 17–21. Best agreement is achieved with heave displacements, while a lower frequency component is predicted in the simulated results for surge and pitch which was not present in the experiment. A spike occurs in the predicted acceleration record between 20 and 30 sec. because of failure of convergence at instants in the simulation; this causes rapid changes in the displacemnet record until dynamic equilibrium is restored. The program recovers from such failures and solutions are continued which, because of damping, again approach steady-state conditions. Tether tensions are underpredicted.

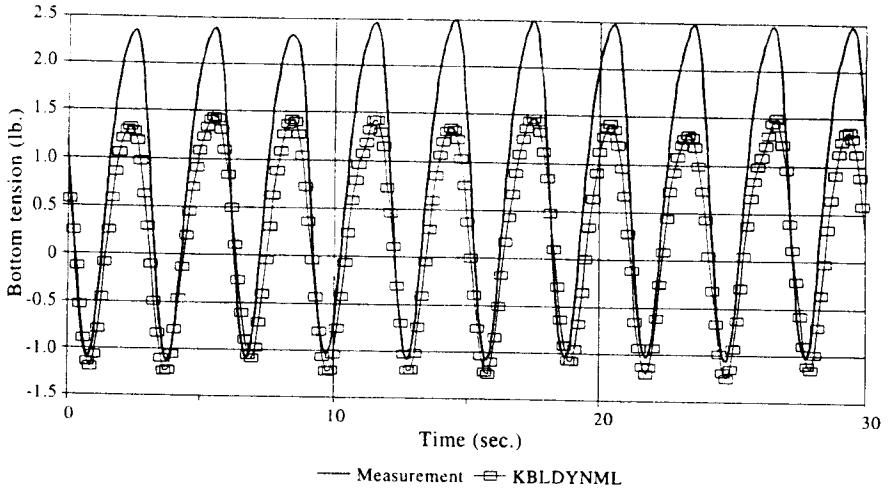

Fig. 21. Bottom tension, disc buoy H=2.5 ft, T=3.0 sec.

6. CONCLUDING REMARKS

A method to compute buoy motions coupled with hydrodynamically loaded mooring motions has been developed. The equations of motion of a floating buoy were derived using a small angle assumption. All six degrees of freedom for the buoy are considered. Coupling between translational and rotational degrees of freedom was included. The developed equations of motion then serve as boundary conditions for the cable.

The formulation provides a methodology to solve the coupled cable-buoy problem. The algorithm is based on a cable dynamic algorithm involving large displacements and nonlinear hydrodynamic forces. However, the formulation of the buoy equations of motion assumed small rotational displacement so that not all nonlinearities were preserved.

The methodology was used to predict responses for three types of tethered buoys; disc, sphere and spar buoys. Numerical predictions were compared to experimental results. Each type of buoy was excited by three different regular waves.

The present model predicted translational motions for all regular wave cases which agree fairly well with experimental data. Rotational motion predictions for the spar buoy, although they under predict the magnitude of the rotational motion, show a similar form with the measured one. For the sphere buoy, pitch predictions give larger values than the measured one. This may have been caused by the fact that the wave period is close to the system's pitch resonance period. The predictions for the disc buoy show good agreement with experimental data. All comparisons of the dynamic component of mooring tension, in regular wave cases, show that the present numerical model under predicts the measurements. This condition may be caused by visco-elastic behavior of the surgical tubing in the experiment. This could not be predicted by the cable algorithm.

Some problems were encountered during computation. Some response predictions show occasional spikes along the time histories because of the effort required by the computer program to recover from a non-convergent solution which occurs during computations.

The present study can be extended in several ways. Implementation of a visco-elastic cable model may provide a better numerical model to predict cable-buoy motion. Equations

of motion for the buoy based on a large angle formulation can be developed and incorporated with the present model so that all nonlinearities in the system are preserved. An alternative approach in the numerical algorithm to couple buoy and cable problem would be desirable such that more stable computations can be obtained and non-convergent solutions discarded.

Acknowledgements—This research was based on support by the Naval Facilities Engineering Service Center, Contract Nos N4708-90-C-1146 and N4708-94-C-7431 and by the Office of Naval Research, Contract No. N00014-92-J-1221.

REFERENCES

Atkinson, K.E. 1989. *An Introduction to Numerical Analysis*, 2nd Ed., John Wiley and Sons, New York.
Bai, K.J. 1977. Zero Frequency Hydrodynamic Coefficients of Vertical Axisymmetric Bodies at a Free Surface. *Journal of Hydronautics*.
Chiou, R., and Leonard, J.W. 1991. Nonlinear Hydrodynamic Response of Curved, Singly-Connected Cables. Proceedings, 2nd International Conference on Computer Modelling in Ocean Engineering, Barcelona, Spain,.
Clough, R.W., and Penzien, J. 1993. 2nd ed., *Dynamics of Structures*, McGraw-Hill, New York.
Jenkins, C.H., Leonard, J.W., Walton, J.S. and Carpenter, E.B. 1995. Experimental investigation of moored-buoys using advanced video techniques. *Ocean Engineering* **22**, 317–335.
Lamb, H., 1945, *Hydrodynamics*, Dover Publications, New York.
Leonard, J.W. and Nath, J.H. 1981. Comparison of finite element and lumped parameter methods for oceanic cables. *Engineering Structures* **3**, 153–167.
Liaw, C.Y., Shankar, N.J. and Chua, K.S. 1989. Large motion analysis of compliant structures using Euler parameters. *Ocean Engineering* **16**, 545–557.
Morison, J.R., O'Brien, M.P., Johnson, J.W. and Schaaft, S.A. 1950. The force exerted by surface waves on piles. *Petroleum Transactions, AIME* **189**, 149–154.
Newmark, M.N. 1959. A Method of Computation for Structural Dynamics. *Journal of the Engineering Mechanic Division, Proceedings ASCE*, July, pp. 67-94.
Nath, J.H., and Thresher, R.W. 1975. Anchor—Last Deployment for Buoy Moorings. *Proceedings, Seventh Offshore Technology Conference*, Houston, TX, Paper OTC 2364.
Patel, M.H. and Lynch, E.J. 1983. Coupled dynamics of tensioned buoyant platforms and mooring tethers. *Engineering Structures* **5**, 299–308.
Webster, R. L. 1975., Nonlinear Static and Dynamic Response of Underwater Cable Structures Using the Finite Element Method, *Proceedings, Seventh Offshore Technology Conference*, Houston, Tx, Paper OTC 2322.

APPENDIX

In this appendix expressions of external forces and moments for small angle formulation are provided. Essentially the appendix provides detailed expressions for buoy equations of motion, Equation (16). The moments applied to the buoy are evaluated at the center of gravity. Hydrodynamic forces and moments are considered as infinitesimal forces/moments components which are integrated over the wetted buoy. Added mass components are included in the mass matrix of the buoy equation of motion and the right hand side of Equation (16) can be expressed as

$$[M]\ddot{\underline{q}} = \begin{bmatrix} M+A_{11} & 0 & 0 & 0 & 0 & 0 \\ 0 & M+A_{22} & 0 & 0 & 0 & A_{26} \\ 0 & 0 & M+A_{33} & 0 & A_{53} & 0 \\ 0 & 0 & 0 & I_{11} & 0 & 0 \\ 0 & 0 & A_{53} & 0 & I_{22}+A_{55} & 0 \\ 0 & A_{62} & 0 & 0 & 0 & I_{33}+A_{66} \end{bmatrix} \begin{Bmatrix} \ddot{x}_1 \\ \ddot{x}_2 \\ \ddot{x}_3 \\ \ddot{\theta}_1 \\ \ddot{\theta}_2 \\ \ddot{\theta}_3 \end{Bmatrix} \tag{A1}$$

where M is mass of the buoy and $I_{(ii)}$ is moment of inertia. $A_{(ij)} = p\ V_{WET}\ C_{A(ij)}$, in which p is

water density; V_{WET} is wetted volume; and $C_{A(i)(j)}$ is the added mass coefficient in the x_i direction due to motion in the x_j direction. Added inertia terms for rotational motion and coupled motions can be defined as follows:

$$M_{A55} = M_{A66} = \int z_1^2 C_A(z_1) A(z_1)\, dz_1 \tag{A2}$$

$$M_{A26} = M_{A62} = M_{A35} = M_{A53} = \int_l z_1 C_A(z_1) A(z_1)\, dz_1$$

Bai (1977) used a finite element method to calculate added inertia coefficients for heave, pitch and coupled pitch-surge motion. The floating bodies of Bai's work are spheroids with slenderness ratios (maximum radius to draft ratio) ranging from 0.1 to 10.0 Bai's results can be incorporated herein since this study considered only axisymetric buoys. The surge added mass coefficient for an infinite fluid is adopted from Lamb (1945). Added mass coefficients for buoys with slenderness ratios between 0.1 and 10.0 can be obtained by linearly interpolating between values from Bai's and Lamb's studies. Bai's added mass inertia coefficients were computed assuming the center of rotation at the water plane. Thus, they must be converted to the center of gravity before being used in the computer program.

$$C_{A26} = \mu_{26} r_w + z_G \mu_{22} \tag{A3}$$

$$C_{A66} = \mu_{66} r_w^2 + 2 z_G \mu_{26} r_w + z_G^2 \mu_{22}$$

Drag forces are assumed acting at the instantaneous center of buoyancy. Drag moments can be obtained from a cross product of drag forces with its moment arm which is the distance from the assumed center of rotation to the center of buoyancy. Then the vector of drag forces and moments can be written as

$$\begin{Bmatrix} \underline{F_d} \\ \underline{N_d} \end{Bmatrix} = \begin{Bmatrix} N_{D1}(u_1 + v_1 - \dot{x}_1) \\ N_{D2}(u_2 + v_2 - \dot{x}_2) \\ N_{D3}(u_3 + v_3 - \dot{x}_3) \\ 0 \\ Z_{GB1} N_{D3}(u_3 + v_3 - \dot{x}_3) \\ Z_{GB1} N_{D2}(u_2 + v_2 - \dot{x}_2) \end{Bmatrix} \tag{A4}$$

where $N_{D(i)} = p\, A_{D(i)} C_{D(i)} Q/2$, in which $A_{D(i)}$ is the drag area; $C_{D(i)}$ the drag coefficient in the x_i direction; and Q the magnitude of $(u_i + v_i - \dot{x}_{Bi})$.

Consider Froude–Kryloff forces acting on an infinitesimal surface of the buoy. The total force can be obtained from integration along the wetted surface. The moment arm is the distance from center of gravity to the particular infinitesimal force. Integration along the wetted surface yields the total excitation forces and moments vector

$$\begin{Bmatrix} \underline{F_K} \\ \underline{N_K} \end{Bmatrix} = \begin{Bmatrix} \rho(1 + C_{A11}) V_{WET} \dot{u} \\ \rho(1 + C_{A22}) V_{WET} \dot{v} \\ \rho(1 + C_{A33}) V_{WET} \dot{w} \\ 0 \\ \rho Z_{GB1} V_{WET} \dot{w} + \rho C_{A53} V_{wet} \dot{w} \\ \rho Z_{GB1} V_{WET} \dot{v} + \rho C_{A62} V_{wet} \dot{v} \end{Bmatrix} \tag{A5}$$

The buoyancy acts at the center of buoyancy in opposition to the weight. The restoring moment for an inclined buoy follows from the moment of excess buoyancy and moment due to the change

of immersion. There is no inertia coupling in this case since the center of rotation is assumed to be at the center of gravity. The buoyancy vector for Equation (16) can be written as

$$\begin{Bmatrix} \underline{B} \\ \underline{N_B} \end{Bmatrix} = \begin{Bmatrix} \rho g V_{\mathrm{WET}} \\ 0 \\ 0 \\ 0 \\ \rho g V_{\mathrm{WET}} Z_{GB1} \theta_2 - \rho g I_{WP}(\theta_2 - \zeta_2) \\ \rho g V_{\mathrm{WET}} Z_{GB1} \theta_3 - \rho g I_{WP}(\theta_3 - \zeta_3) \end{Bmatrix} \tag{A6}$$

where θ_i is the buoy instantaneous angle and ζ_i is the angle of wave slope.

The tension components at the connection point are formulated in the global coordinate system so that they can be directly applied in Equation (16). Moments caused by tether tensions are evaluated at the center of gravity. External force and moment vectors due to tether tension can be written as

$$\begin{Bmatrix} \underline{T} \\ \underline{N_T} \end{Bmatrix} = \begin{Bmatrix} T_1 \\ T_2 \\ T_3 \\ (z_{T2} - \theta_1 z_{T3} + \theta_3 z_{T1}) T_3 + (-z_{T3} - \theta_1 z_{T2} + \theta_2 z_{T1}) T_2 \\ (z_{T3} + \theta_1 z_{T2} - \theta_2 z_{T1}) T_1 + (-z_{T1} - \theta_2 z_{T3} + \theta_3 z_{T2}) T_3 \\ (-z_{T2} + \theta_1 z_{T3} - \theta_3 z_{T1}) T_1 + (z_{T1} + \theta_2 z_{T3} - \theta_3 z_{T2}) T_2 \end{Bmatrix} \tag{A7}$$

The Jacobian matrices in Section 4 are obtained as partial derivatives of the above equations with respect to the various dependent variables. They are tabulated below:

$$J^*_{Fxil} = \frac{\partial f^*_i}{\partial \dot{x}_{Tl}} = \frac{M_{(i)} + \rho V_{\mathrm{wet}} C_{A(i)(i)}}{\alpha \Delta t} \delta_{il} - N^*_{D(i)} \delta_{il} - \frac{\partial N^*_{D(i)}}{\partial \dot{X}_{Tl}} (u_i + v_i - \dot{x}^*_{Ti} - \epsilon_{ijk} z_{TBk} \dot{\theta}^*_j) \tag{A8}$$

$$J^*_F \theta_{il} = \frac{\partial f^*_i}{\partial \dot{\theta}_l} = M_{(i)} + \rho V_{\mathrm{wet}} C \frac{C_{A(i)(i)}}{\alpha \Delta t} \epsilon_{ijk} z_{Tk} \delta_{jl} - \frac{\rho V_{\mathrm{wet}} C_{A(i)(j+3)}}{\alpha \Delta t} \delta_{jl} - N^*_{D(i)} \epsilon_{ijk} z_{TBk} \delta_{jl} \tag{A9}$$
$$- \frac{\partial N^*_{D(i)}}{\partial \theta_l} (u_i + v_i - \dot{x}^*_{Ti} - \epsilon_{ijk} z_{TBk} \dot{\theta}^*_j)$$

$$J^*_{FTil} = \frac{\partial f^*_i}{\partial T_l} = -\delta_{il} \tag{A10}$$

$$J^*_H \theta_{il} = \frac{\partial h^*_i}{\partial \dot{\theta}_l} = \frac{I_{ij} + \rho V_{\mathrm{wet}} C_{A(i+3)(j+3)}}{\alpha \Delta t} \delta_{jl} - \frac{\rho V_{\mathrm{wet}} C_{A(i+3)(j)}}{\alpha \Delta t} \epsilon_{ijk} z_{Tk} \delta_{jl} - \frac{\partial N^*_{D(i)}}{\partial \theta_l} W_{ij} \dot{x}^*_{Tj}$$
$$- \frac{\partial N^*_{D(k)}}{\partial \theta_l} \epsilon_{kjn} z_{TBn} W_{ik} \dot{\theta}^*_j - N^*_{D(k)} \epsilon_{kjn} z_{TBn} W_{ik} \delta_{jl} + [z_{Wi} F_{Wj} - z_{Ti} T^*_j + z_{Bi} B_j \delta_{1j} \tag{A11}$$
$$- \rho g I_{wpi} \alpha \Delta t \delta_{jl} - \delta_{ij} (z_{Wk} F_{Wk} - z_{GTk} T_k + z_{BGk} B_k \delta_{1k})] \alpha \Delta t \delta_{jl}$$
$$- \epsilon_{ijk} \frac{\partial N^*_{D(k)}}{\partial \theta_l} z_{Bj} (u_k + v_k)$$

$$J^*_{HTil} = \frac{\partial h^*_i}{\partial T_l} = [-z_{GTi} \delta_{jl} - \delta_{ij} (-z_{GTk} \delta_{kl})] \alpha \Delta t \theta^*_j - \epsilon_{ijk} z_{GTj} \delta_{kl} \tag{A12}$$

$$J^*_{Hxil} = \frac{\partial h^*_i}{\partial \dot{x}_{Tl}} = \frac{\rho V_{\mathrm{wet}} C_{A(i+3)(j)}}{\alpha \Delta t} \delta_{il} - \frac{\partial N^*_{D(i)}}{\partial \dot{X}_{Tl}} W_{ij} \dot{x}_{Tj} - N^*_{D(k)} W_{ij} \delta_{jl} \tag{A13}$$
$$- \frac{\partial N^*_{D(k)}}{\partial \dot{X}_{Tl}} \epsilon_{kjn} z_{TBn} W_{ik} \dot{\theta}^*_j - \epsilon_{ijk} \frac{\partial N^*_{D(k)}}{\partial \dot{X}_{Tl}} z_{Bj} (u_k + v_k)$$